

Gradient corrections to the kinetic energy density functional of a two-dimensional Fermi gas at finite temperature

B. P. van Zyl⁽¹⁾, K. Berkane⁽²⁾, K Bencheikh⁽²⁾, A. Farrell⁽¹⁾

¹*Department of Physics, St. Francis Xavier University,
Antigonish, NS, Canada B2G 2W5 and*

²*Département de Physique. Laboratoire de physique quantique et
systèmes dynamiques. Université de Sétif, Setif 19000, Algeria.*

(Dated: June 17, 2022)

Abstract

We examine the leading order semiclassical gradient corrections to the non-interacting kinetic energy density functional of a two dimensional Fermi gas by applying the extended Thomas-Fermi theory at finite temperature. We find a non-zero von Weizsäcker-like gradient correction, which in the high-temperature limit, goes over to the familiar functional form $(\hbar^2/24m)(\nabla\rho)^2/\rho$. Our work provides a theoretical justification for the inclusion of gradient corrections in applications of density-functional theory to inhomogeneous two-dimensional Fermi systems at any *finite* temperature.

PACS numbers: 71.15.Mb,03.65.Sq,05.30.Fk,31.15.Bs

I. INTRODUCTION

In 1966, Fowler *et al.*¹ performed transport measurements on a Si-metal-oxide-semiconductor structure in which a degenerate gas of electrons was electrostatically induced. Their work demonstrated for the first time that the density of states in the n -type electron inversion layer had the expected behaviour for a two-dimensional electron gas (2DEG). Since Fowler's seminal work, the exploitation of the electronic properties of III-V semiconductors has led to the realization of high quality, high mobility 2DEG's at the interface of epitaxially grown III-V structures, such as GaAs/AlGaAs heterostructures.² Through electrostatic, and/or etching techniques, the 2DEG found in the III-V semiconductor interface, can be manipulated to create experimental realizations of low dimensional electron systems such as quantum wires, quantum dots and quantum anti-dots.

By far, the workhorse for a theoretical understanding of the bulk electronic properties of such low-dimensional electronic systems is the zero-temperature ($T = 0$) density-functional theory (DFT) of Hohenberg, Kohn and Sham (HKS).^{3,4} The key element in the HKS approach is the definition of the kinetic energy (KE), corresponding to a system of N noninteracting fermions moving in some effective one-body potential. The HKS scheme treats the KE *exactly* at the independent particle level, and so the development of explicit, orbital-free functionals for $\mathcal{T}[\rho]$, the KE density functional, is an important objective. Ideally the appropriate functional should yield both the correct energy *and* the correct density profile.

To this end, the simplest approach for the construction of the KE density functional, $\mathcal{T}[\rho]$, is the local-density approximation (LDA), sometimes referred to as the Thomas-Fermi (TF) approximation.^{5,6} In this approximation, the density of each infinitesimal region of the *inhomogeneous* electron gas is taken to be precisely equal to the density of a *homogeneous* electron gas with the same density as the corresponding infinitesimal volume element. One would then expect the LDA to be applicable only in cases where the density in the system is a slowly varying function of position. In fact, this is not the case, and even in highly inhomogeneous systems, the LDA is found to work reasonably well.^{7,8}

Although the LDA for the KE density leads to reasonable results for the energy, the calculated density profile in a self-consistent DFT scheme does not exhibit the desired quantum mechanical tunnelling into the classically forbidden region. To overcome this issue, the so-called von Weizsäcker (vW) gradient correction,⁹ $\propto (\nabla\rho)^2/\rho$, is added to the KE functional. In 3D, the vW gradient correction can be rigorously justified within the extended TF (ETF) theory, originally

developed in the context of nuclear physics.¹⁰ The inclusion of the vW term leads to smooth and continuous densities, while improving the quality of the KE functional by taking into account the inhomogeneity of the system.

An application of the ETF theory to 2D systems, however, leads to the conclusion that there are *no gradient corrections* to the 2D KE density functional.¹¹⁻¹³ This, of course, makes no physical sense since the LDA cannot be variationally exact for an inhomogeneous system. Thus in DFT applications to systems derived from the inhomogeneous 2DEG discussed above, a phenomenological approach must be taken in which a vW-like gradient correction is put in “by hand”.¹⁴ Although the vW-like correction term is entirely *ad hoc* for a 2D system, its use has been justified by (i) the KE reduces to the TF limit for slowly varying densities, and (ii) it allows one to represent strongly inhomogeneous densities in a quantum mechanically reasonable way.

To date, there has been no formal justification for the inclusion of a vW-like term for 2D systems at zero-temperature. In this paper, we establish the existence of a vW-like gradient correction to the 2D KE density functional at *finite temperatures*. Our approach parallels the earlier work of Brack¹⁵, in which the ETF theory was developed in the context of “hot” nuclear matter (ETFT). Given the recent work of Eschrig,¹⁶ which aims at providing a rigorous foundation for DFT at finite-temperature, the results presented in this paper are immediately relevant to future applications of $T > 0$ DFT in low dimensional electronic systems.

The rest of our paper is organized as follows. In the next section we provide a brief review of the general ETFT approach, followed by an explicit calculation of the $T > 0$ second order gradient correction to the 2D KE functional. In Sec. III we numerically investigate the quality of the gradient corrected functional by comparing it to known, exact results, for an isotropic 2D harmonic oscillator at finite temperature. The paper concludes in Sec. IV with a brief summary and suggestions for future investigations.

II. EXTENDED THOMAS-FERMI THEORY AT FINITE-TEMPERATURE

In this section, we provide a brief review of the ETFT approach. The interested reader should refer to the Ref. [10] for a detailed discussion of the ETFT and the Wigner-Kirkwood semiclassical expansion.

A. Spatial density

At the heart of the ETFT approach is the Wigner-Kirkwood semiclassical expansion of the zero-temperature, diagonal Bloch density matrix (BDM), which in 2D is given by¹⁰

$$C_0(\mathbf{r}; \beta) = \left(\frac{1}{\lambda}\right)^2 e^{-\beta V(\mathbf{r})} \left(1 - \frac{\hbar^2 \beta^2}{12m} \left[\nabla^2 V - \frac{\beta}{2}(\nabla V)^2\right] + \dots\right), \quad (1)$$

where $V(\mathbf{r})$ is a local one-body potential, and for our purposes, we have only shown terms up to relative order \hbar^2 and $\lambda \equiv (2\pi\hbar^2\beta/m)^{1/2}$. Note that β is to be viewed as a complex parameter here, and not the inverse temperature $1/(k_B T)$. In order to incorporate finite temperatures into the WK semiclassical theory, the finite-temperature BDM is defined by¹⁵

$$C_T(\mathbf{r}; \beta) \equiv C_0 \frac{\pi\beta k_B T}{\sin(\pi\beta k_B T)}. \quad (2)$$

The finite-temperature spatial density is then obtained from an (all two-sided) inverse Laplace transform (ILT) of the finite-temperature BDM, *viz.*,

$$\rho(\mathbf{r}; T) = \mathcal{L}_\mu^{-1} \left[2 \frac{C_T(\mathbf{r}; \beta)}{\beta} \right], \quad (3)$$

where the factor of two in Eq. (3) accounts for the spin degeneracy after the spin trace has been taken, and μ has the physical significance of the chemical potential. In what follows, we will make use of the following ILTs:

$$\mathcal{L}_\mu^{-1} \left[\beta^n e^{-\beta V} \frac{\pi k_B T}{\sin(\pi\beta k_B T)} \right] = \int_{-\infty}^{\infty} \delta^{(n)}(\tau) \frac{1}{e^{\tau/k_B T} z^{-1} + 1} d\tau, \quad (n \geq 0) \quad (4)$$

$$\mathcal{L}_\mu^{-1} \left[\beta^{-1} e^{-\beta V} \frac{\pi k_B T}{\sin(\pi\beta k_B T)} \right] = \int_0^{\infty} \frac{1}{e^{\tau/k_B T} z^{-1} + 1} d\tau = k_B T \ln(1+z) \quad (5)$$

$$\mathcal{L}_\mu^{-1} \left[\beta^{-2} e^{-\beta V} \frac{\pi k_B T}{\sin(\pi\beta k_B T)} \right] = \int_0^{\infty} \frac{\tau}{e^{\tau/k_B T} z^{-1} + 1} d\tau = -(k_B T)^2 \text{Li}_2(-z) \quad (6)$$

where $\text{Li}_2(\cdot)$ is the polylog function,¹⁷ and $z \equiv \exp[(\mu - V)/k_B T]$. Using Eq. (3), along with Eqs. (4–6), readily leads to the following second-order expression for the finite-temperature spatial density:

$$\begin{aligned} \rho(\mathbf{r}; T) &= \left(\frac{mk_B T}{\pi\hbar^2}\right) \ln(1+z) - \frac{(\nabla V)^2}{24\pi k_B^2 T^2} \frac{z(z-1)}{(z+1)^3} - \frac{\nabla^2 V}{12\pi k_B T} \frac{z}{(z+1)^2} \\ &= \rho^{(0)}(\mathbf{r}; T) + \rho^{(2)}(\mathbf{r}; T). \end{aligned} \quad (7)$$

The ETFT density in Eq. (7) is well-defined throughout all space, with the last two terms, denoted by $\rho^{(2)}(\mathbf{r}; T)$, being relative order \hbar^2 greater than the first term, $\rho^{(0)}(\mathbf{r}; T)$. Note that in Eq. (7), for

$V(\mathbf{r}) < \mu$, $z \rightarrow \infty$ exponentially as $T \rightarrow 0$, so that the $T \rightarrow 0$ limit is well-defined only *within the classical region*; the non-analytic behaviour of the zero-temperature ETF densities at the turning point, $\mu = V(\mathbf{r})$, is well-known.¹⁰ What we find here is that the singular behaviour of the $T = 0$ densities cannot be avoided by first formulating the semiclassical theory at finite-temperature, and then performing the $T \rightarrow 0$ limit.¹⁸ We have, however, confirmed that the $T \rightarrow 0$ limit of Eq. (7) with $V(\mathbf{r}) < \mu$ correctly reduces to the known (albeit problematic) $T = 0$ result.¹⁰

B. Kinetic energy density

The kinetic energy density may be evaluated from¹⁵

$$\mathcal{T}(\mathbf{r}; T) = -\rho(\mathbf{r}; T)V(\mathbf{r}) + \mathfrak{F}(\mathbf{r}; T) + T\sigma(\mathbf{r}; T), \quad (8)$$

where

$$\mathfrak{F}(\mathbf{r}; T) = \mu\rho(\mathbf{r}; T) - \mathcal{L}_\mu^{-1} \left[\frac{C_T}{\beta^2} \right], \quad (9)$$

is the free energy density, and

$$\sigma(\mathbf{r}; T) = \frac{\partial}{\partial T} \mathcal{L}_\mu^{-1} \left[\frac{C_T}{\beta^2} \right], \quad (10)$$

is the entropy density. Each of the contributions to $\mathcal{T}(\mathbf{r}; T)$ can be easily determined to second-order following the same method as for the spatial density. A straightforward calculation results in the following expression for the finite-temperature KE density

$$\begin{aligned} \mathcal{T}(\mathbf{r}; T) &= -\frac{mk_B^2 T^2}{\pi \hbar^2} \text{Li}_2(-z) - \frac{z(\nabla V)^2}{12\pi k_B T(z+1)^2} + \frac{\nabla^2 V}{12\pi} \frac{z}{z+1} \\ &\equiv \mathcal{T}^{(0)}(\mathbf{r}; T) + \mathcal{T}^{(2)}(\mathbf{r}; T), \end{aligned} \quad (11)$$

where, following Eq. (7), the last two terms in Eq. (11) are denoted collectively by $\mathcal{T}^{(2)}(\mathbf{r}; T)$. As in Eq. (7), the $T \rightarrow 0$ limit of Eq. (11) is well-defined only within the classical region.

C. Second-order kinetic energy density functional

For the special case of 2D, the elimination of z and V in $\mathcal{T}(\mathbf{r}; T)$ above, in favour of the spatial density, ρ , is quite straightforward.^{18–20} To begin we define $\tilde{V} \equiv \frac{\mu-V}{k_B T}$, so that $z = \exp(\tilde{V})$. Thus, the density, Eq. (7), is a function of \tilde{V} , $\nabla \tilde{V}$ and $\nabla^2 \tilde{V}$. Calculating from Eq. (7) $\nabla \rho$ and $\nabla^2 \rho$ and consistently neglecting higher than second derivatives of the potential, we have: $\rho =$

$\rho(\tilde{V}, \nabla\tilde{V}, \nabla^2\tilde{V})$, $\nabla\rho = \nabla\rho(\cdot \cdot \cdot)$, and $\nabla^2\rho = \nabla^2\rho(\cdot \cdot \cdot)$, which can be solved for \tilde{V} , $\nabla\tilde{V}$ and $\nabla^2\tilde{V}$; inserting this into Eq. (11) yields the finite-temperature kinetic energy density functional up to $\mathcal{O}(\hbar^2)$, *viz.*,

$$\begin{aligned}\mathcal{T}_{\text{ETFT}}[\rho] &= -A_T k_B T \text{Li}_2(1 - e^{\rho/A_T}) - \frac{\hbar^2}{12m} \nabla^2\rho - \frac{\hbar^2}{12m} f_1(\mathbf{r}; T) \nabla^2\rho \\ &+ \frac{\hbar^2}{24m} f_2(\mathbf{r}; T) \frac{(\nabla\rho)^2}{\rho} \\ &= \mathcal{T}_{\text{TFT}}[\rho] + \mathcal{T}_{\text{ETFT}}^{(2)}[\rho],\end{aligned}\quad (12)$$

where

$$f_1(\mathbf{r}; T) = \frac{\rho}{A_T(e^{\rho/A_T} - 1)}, \quad (13)$$

$$f_2(\mathbf{r}; T) = e^{\rho/A_T} [f_1(\mathbf{r}; T)]^2, \quad (14)$$

and $A_T \equiv mk_B T / (\pi\hbar^2)$. The first term in Eq. (12) is the finite-temperature 2D TFT KE density functional, $\mathcal{T}_{\text{TFT}}[\rho]$, while the other three terms represent the $\mathcal{O}(\hbar^2)$ gradient corrections. As advertised, the last term in Eq. (12) has the vW form $\sim (\nabla\rho)^2/\rho$.

An alternative expression for the KE functional may also be given, *viz.*,

$$\begin{aligned}\mathcal{T}_{1,\text{ETFT}}[\rho] &= -A_T k_B T \text{Li}_2(1 - e^{\rho/A_T}) + \frac{\hbar^2}{6m} \nabla^2\rho - \frac{\hbar^2}{12m} f_1(\mathbf{r}; T) \nabla^2\rho \\ &+ \frac{\hbar^2}{24m} f_2(\mathbf{r}; T) \frac{(\nabla\rho)^2}{\rho},\end{aligned}\quad (15)$$

which is obtained by making use of the well-known connection between $\mathcal{T}[\rho]$ and $\mathcal{T}_1[\rho]$ in the presence of time-reversal symmetry:

$$\mathcal{T}_1[\rho] = \mathcal{T}[\rho] + \frac{\hbar^2}{4m} \nabla^2\rho. \quad (16)$$

Both $\mathcal{T}_{\text{ETFT}}[\rho]$ and $\mathcal{T}_{1,\text{ETFT}}[\rho]$ integrate to the same total kinetic energy for finite systems.

To investigate the low temperature behaviour of Eqs. (12) and (15) we use,

$$\lim_{\rho/A_T \rightarrow \infty} \text{Li}_2(-e^{\rho/A_T}) = -\frac{1}{2} \left(\frac{\rho}{A_T} \right)^2, \quad (17)$$

along with the fact that $f_1(\mathbf{r}; T) \rightarrow 0$, and $f_2(\mathbf{r}; T) \rightarrow 0$ as $T \rightarrow 0$, to write

$$\mathcal{T}_{\text{ETFT}}[\rho] \rightarrow \frac{\hbar^2}{2m} \left(\pi\rho^2 - \frac{1}{6} \nabla^2\rho \right), \quad (18)$$

and

$$\mathcal{T}_{1,\text{ETFT}}[\rho] \rightarrow \frac{\hbar^2}{2m} \left(\pi\rho^2 + \frac{1}{3} \nabla^2\rho \right). \quad (19)$$

Equations (18) and (19) agree with the known results for the $T = 0$ 2D KE functionals $\mathcal{T}[\rho]$ and $\mathcal{T}_1[\rho]$, respectively.¹⁰ As mentioned above, for physical densities, integration over $\nabla^2\rho$ vanishes. Therefore, in any practical implementation of self-consistent $T = 0$ DFT, the Laplacian term may be ignored, and we may write

$$\mathcal{T}_{\text{ETFT}}[\rho] = \mathcal{T}_{1,\text{ETFT}}[\rho] = \frac{\hbar^2}{2m} (\pi\rho^2) , \quad (20)$$

as $T \rightarrow 0$. We see that there is no vW-like gradient correction at $T = 0$, leading to the incorrect conclusion that for an inhomogeneous 2D Fermi gas, the TF KE functional (at least to second-order) is exact.²¹

It is readily found that as $T \rightarrow \infty$, $f_1(\mathbf{r}; T) \rightarrow 1$ and $f_2(\mathbf{r}; T) \rightarrow 1$, so that up to $\mathcal{O}(\hbar^2)$, the 2D KE functionals go over to

$$\mathcal{T}_{\text{ETFT}}[\rho] \rightarrow \mathcal{T}_B[\rho] = k_B T \rho - \frac{\hbar^2}{6m} \nabla^2 \rho + \frac{\hbar^2}{24m} \frac{(\nabla \rho)^2}{\rho} , \quad (21)$$

and

$$\mathcal{T}_{1,\text{ETFT}}[\rho] \rightarrow \mathcal{T}_{1,B}[\rho] = k_B T \rho + \frac{\hbar^2}{12m} \nabla^2 \rho + \frac{\hbar^2}{24m} \frac{(\nabla \rho)^2}{\rho} . \quad (22)$$

Therefore, at high-temperature, the second order gradient corrections take the familiar functional form found in 3D ETF, although the numerical pre-factors are different. It is also interesting to note that the high-temperature limit of the TFT term is linear in the density, $k_B T \rho$, in contrast to the quadratic dependence, $\pi\rho^2/2$, exhibited in the zero-temperature limit. We have also checked that the high-temperature limit of the 2D KE functional may be obtained by performing an analogous calculation assuming a Boltzmann, rather than a Fermi, gas.

III. COMPARISON WITH EXACT RESULTS

In a previous study, Brack and van Zyl²² examined the $T = 0$ 2D TF KE functional by comparing its global (*i.e.*, integrated) and local (*i.e.*, spatially dependent) properties with the known analytical expressions for the 2D harmonic oscillator (HO) potential. They found the remarkable result that at $T = 0$, the 2D TF KE functional (*without gradient corrections*), when using the exact spatial density of the 2D HO, gives the exact quantum mechanical kinetic energy. This result is highly non-trivial because the TF functional is simply the LDA to the true KE, and therefore, cannot be variationally exact. More surprising, however, is how well the local behaviour of the exact KE density is reproduced by the TF approximation, as illustrated in Fig. 3 of Ref. [22]. The

purpose of this section is to perform an analogous calculation for the finite-temperature KE density functionals presented in this paper. In our numerical calculations, we have scaled all energies and lengths by $\hbar\omega$, and $\ell_{\text{osc}} = \sqrt{\hbar/m\omega}$, respectively. We have also restricted our attention to relatively small particle numbers, N , since it can be shown rigorously that in the large- N limit, the TF approximation becomes exact.²³

The finite-temperature kinetic energy densities are calculated *via*²⁴

$$\mathcal{T}_{\text{exact}}(\mathbf{r}; T) = -\frac{1}{2} \left(\frac{1}{4} \nabla_{\mathbf{r}}^2 + \nabla_{\mathbf{s}}^2 \right) \rho_{\text{exact}}(\mathbf{r}, \mathbf{s}; T)|_{\mathbf{s}=0}, \quad (23)$$

$$\mathcal{T}_{1,\text{exact}}(\mathbf{r}; T) = \frac{1}{2} \left(\frac{1}{4} \nabla_{\mathbf{r}}^2 - \nabla_{\mathbf{s}}^2 \right) \rho_{\text{exact}}(\mathbf{r}, \mathbf{s}; T)|_{\mathbf{s}=0}, \quad (24)$$

where specializing to the case of the 2D HO,

$$\rho_{\text{exact}}(\mathbf{r}, \mathbf{s}; T) = \frac{2}{\pi} \sum_{n=0}^{\infty} \sum_{k=0}^{\infty} (-1)^n L_n(2r^2) L_k(s^2/2) e^{-(r^2+s^2/4)} \frac{1}{\exp(\frac{n+1+k-\mu}{T}) + 1}, \quad (25)$$

is the *exact* finite-temperature first-order density matrix. Putting $\mathbf{s} = 0$ in Eq. (25) gives the exact finite-temperature particle density for the 2D HO, *viz.*,

$$\rho_{\text{exact}}(\mathbf{r}; T) = \frac{2}{\pi} \sum_{n=0}^{\infty} \sum_{k=0}^{\infty} (-1)^n L_n(2r^2) e^{-r^2} \frac{1}{\exp(\frac{n+1+k-\mu}{T}) + 1}. \quad (26)$$

In Table I below, we present a numerical comparison of the kinetic energies as obtained from

$$K_{\text{exact}} = \int \mathcal{T}_{\text{exact}}(\mathbf{r}) d^2r, \quad \text{c.f. Eq. (23)} \quad (27)$$

$$K_{\text{TFT}} = \int \mathcal{T}_{\text{TFT}}[\rho_{\text{exact}}] d^2r, \quad \text{c.f. Eq. (12)} \quad (28)$$

$$K_{\text{ETFT}} = \int \mathcal{T}_{\text{ETFT}}[\rho_{\text{exact}}] d^2r, \quad \text{c.f. Eq. (12)}, \quad (29)$$

for $N = 42$ particles, with Table II providing the same calculation for $N = 420$ particles.

It is clear that the TFT KE, K_{TFT} , is always lower than the exact KE density, K_{exact} , while the gradient corrections serve to improve the agreement with the exact result. This makes sense given that the gradient corrections take into account the curvature of the system imposed by the external potential, thereby increasing the kinetic energy of the system. It is nevertheless quite surprising how well the TFT functional does in describing the kinetic energy of the strongly inhomogeneous 2D HO at finite temperature, even for small particle numbers. From our numerical calculations, we observe that a ten-fold increase in the number of particles reduces the *largest* relative percentage

T	K_{exact}	K_{TFT}	K_{ETFT}
0.5	93.8637	93.3831	93.6606
0.8	97.8141	97.2737	97.7024
1.0	101.2944	100.7172	101.2162
2.0	125.9627	125.2634	125.9119
3.0	157.7902	157.0672	157.7134
4.0	192.9207	192.2189	192.8126
5.0	229.5101	228.8539	229.3848

Table I: A comparison of the total kinetic energy at various temperatures as determined from Eq (27–29) with $N = 42$ particles. All quantities are measured in scaled units, as discussed in the text. The largest relative percentage errors in our tabulated data are $\Delta K_{\text{TFT}} \sim 0.5\%$ and $\Delta K_{\text{ETFT}} \sim 0.2\%$.

T	K_{exact}	K_{TFT}	K_{ETFT}
0.5	2878.9107	2877.5299	2878.0039
0.8	2892.0023	2890.5957	2891.3984
1.0	2904.0294	2902.5772	2903.5678
2.0	3002.1833	3000.4547	3001.9538
3.0	3157.9352	3155.8726	3157.6062
4.0	3361.3488	3358.9266	3360.8216
5.0	3602.6770	3599.8900	3601.8962

Table II: As in Table I, but with $N = 420$ particles. The largest relative percentage errors in our tabulated data are $\Delta K_{\text{TFT}} \sim 0.06\%$ and $\Delta K_{\text{ETFT}} \sim 0.03\%$.

error by roughly a factor of ten; this trend is in keeping with the known result that in the large- N limit, the TF approximation becomes exact.

In Figs. 1 and 2, we present the KE densities, $\mathcal{T}_{\text{exact}}(\mathbf{r})$, $\mathcal{T}_{\text{TFT}}[\rho]$, and $\mathcal{T}_{\text{ETFT}}[\rho]$ with $N = 42$ particles, at $T = 0.2$ and $T = 2$, respectively. As in Tables I and II, the exact spatial density, Eq. (26), has been used as input for the KE functionals. We have focused on a small number of particles, *viz.*, $N = 42$, since deviations between the exact, TFT, and ETFT densities are more

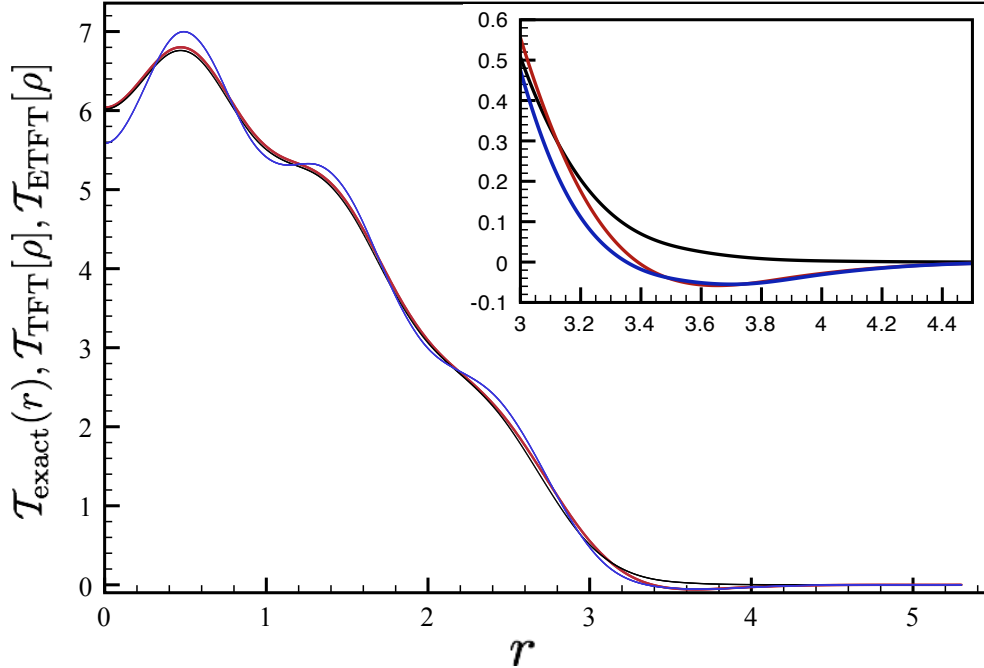


Figure 1: (colour online) A plot of the exact, Eq. (23), TFT, *i.e.*, the first term in Eq. (12), and the ETFT, Eq. (12), KE densities for $N = 42$ particles and $T = 0.2$. The red curve is the exact KE density, the black curve is the TFT KE density, and the blue curve is the ETFT KE density. Inset: Magnification of the tail region, where deviations between the three curves are most pronounced. Scaled units are used, as discussed in the text.

pronounced for $N \lesssim \mathcal{O}(10^2)$, particularly at low temperatures.

Figure 1 reveals several interesting aspects of the level of approximation at low temperatures. First, we note that the TFT (black curve) and the exact KE density (red curve) are almost indistinguishable within $0 < r \lesssim 3$. However, near the tail region (see figure inset), it is clear that the two KE densities are quite different; the TFT density is strictly positive definite, whereas the exact KE density falls below zero, before coalescing with the TFT density for $r \gtrsim 4.5$. The ETFT KE density (blue curve), on the other hand, does a relatively poor job of quantitatively capturing the behaviour of the exact KE density in the interior, but for the tail region, more accurately reproduces the exact result. Indeed, for $r \gtrsim 3.5$, the ETFT and exact KE densities are indistinguishable on the scale of the inset. Moreover, in spite of the differences between the exact and ETFT densities for $r \lesssim 3$, the ETFT is still a better approximation for the total KE, as evidenced by the data presented in Table I. Therefore, while the gradient corrections are important for improving the total (*i.e.*,

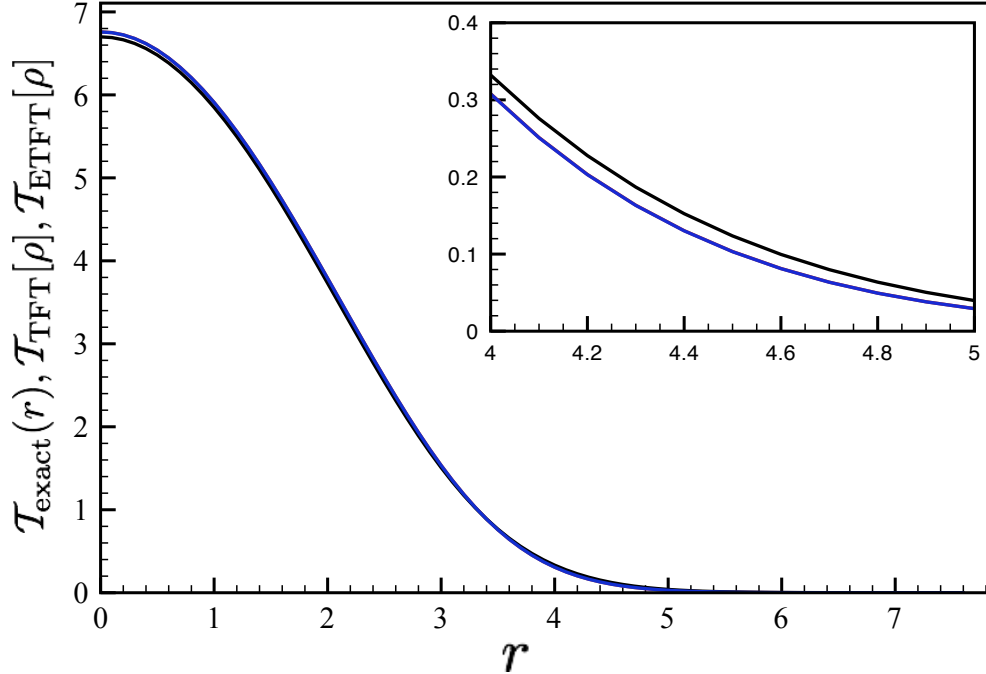


Figure 2: (colour online) As in Fig. 1, but with $T = 2.0$. Note that at this temperature, the shell oscillations are already completely washed away. Inset: Magnification of the tail region, clearly illustrating that the exact (red) and ETFT (blue) curves are indistinguishable on the scale of the plot.

integrated) KE, they are essential for describing the correct behaviour of the exact KE near the classical turning point.

Figure 2 presents the same data as in Fig. 1, but with $T = 2.0$. At this temperature, the shell oscillations are already completely washed out, and the exact and ETFT KE densities are *indistinguishable* from each other, including the tail region; in the inset, there are actually three curves plotted, but the difference between the red (exact) and blue (ETFT) curves cannot be resolved. Thus, at temperatures for which the shell effects are absent (*i.e.*, $T \gtrsim 1$), the ETFT is an excellent approximation to the exact finite-temperature KE density. Near the tail region, we see that the TFT KE density (black) is consistently too large, thereby emphasizing the importance of the gradient corrections for a faithful description of the local behaviour of the exact KE density, even for small particle numbers.

Finally, in Fig. 3, we illustrate the temperature and spatial dependence of the vW coefficient, $f_2(\mathbf{r}; T)$ given by Eq. (14), for $N = 420$ particles, and $N = 42$ (inset). As the temperature is increased, we see that the vW coefficient approaches the constant value $f_2(\mathbf{r}; T) = 1$, confirming

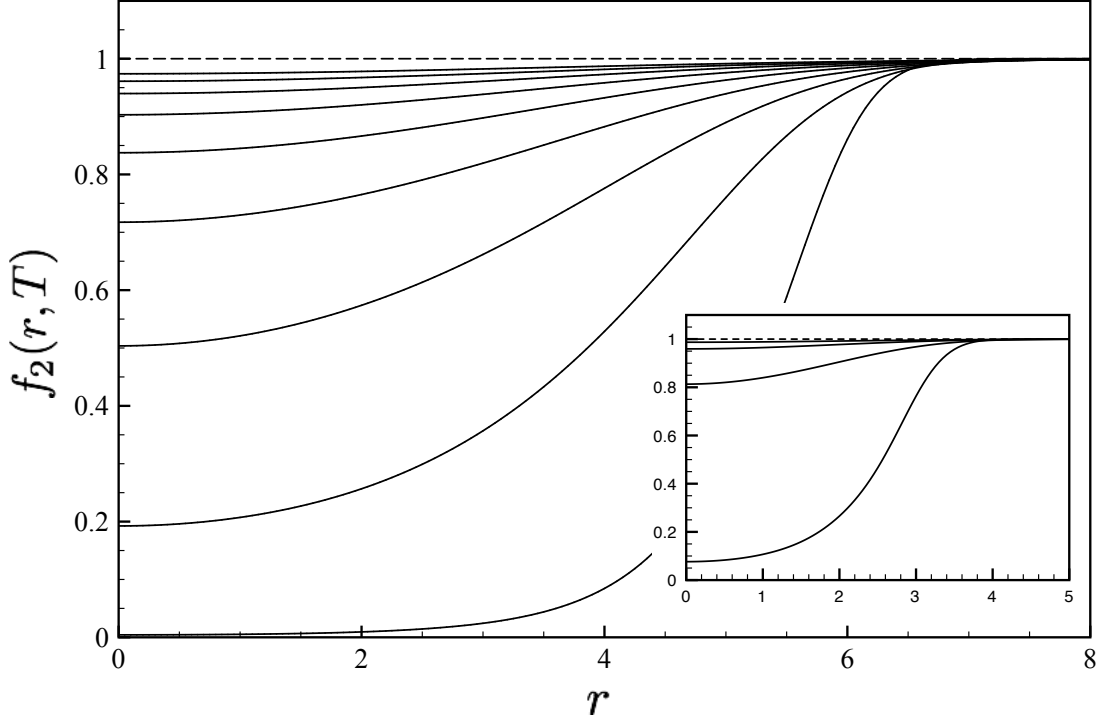


Figure 3: A plot of the coefficient of the von Weizsäcker term, Eq. (14), for $N = 420$ particles. The curves correspond, from lowest to highest, to $T = 2$ and $T = 18$, respectively, in steps of $\Delta T = 2$. Note that by $T = 18$, $f_2(\mathbf{r}; T)$ is already approaching its Boltzmann value, $f_2(\mathbf{r}; T) = 1$, represented by the dashed line. Inset: As in the main figure, but for $N = 42$ particles at temperatures $T = 1, 3, 5, 7$. Scaled units have been used, as discussed in the text.

our analytical results above for the Boltzmann regime. Figure 3 establishes that $T \gtrsim 18$ is a sufficiently high temperature for the $N = 420$ particle system to be treated as Boltzmann gas. The inset illustrates the expected result that for smaller particle numbers, one enters the Boltzmann regime at much lower temperatures.

IV. CONCLUSIONS AND OUTLOOK

We have provided a formal justification for the inclusion of gradient corrections to the 2D KE density functional of an ideal Fermi gas at finite temperatures. Our numerical calculations have examined the quality of the TFT and ETFT functionals by comparing them against exact, analytical results for the 2D HO potential. We find that gradient corrections lead to an improved agreement for total KE when compared to the TFT approximation, and are necessary to correctly

reproduce the quantum mechanical tunneling into the classically forbidden region exhibited by the exact KE density. Unfortunately, the non-analytic behaviour of the $T = 0$ semiclassical densities at the classical turning point cannot be remedied within the present formalism. We hope to resolve the issues surrounding the $T = 0$ 2D semiclassical gradient expansion in the near future.

In a forthcoming work, we will develop the finite-temperature Dirac exchange functional, which we propose to use in a fully self-consistent, finite-temperature Thomas-Fermi-Dirac von Weizsäcker (TFDW) DFT calculation similar to what has already been done at $T = 0$ for low-dimensional Fermi systems.¹⁴ The goal of this study will be to investigate the quality of the TFT and ETFT density functionals for an interacting, strongly inhomogeneous, *e.g.*, quantum dot, many-body Fermi system. We will be particularly interested in the $T \lesssim 1$ regime, so that we may compare the finite-temperature KE functionals presented here against the $T = 0$ TFDW calculations, where the vW gradient correction must be put in by hand. It will be of interest to see whether the optimal, *ad hoc*, $T = 0$ vW coefficient of $1/8$ can be motivated from a finite-temperature self-consistent TFDW calculation.

Finally, we wish to point out that the results presented here may also find relevance in current experiments on ultra-cold, trapped Fermi gases, in which inter-atomic interactions may be tuned from essentially zero, to very strong, *via* the Feshbach resonance.²⁵ It is possible that the low-temperature shell oscillations, and their suppression as the temperature is increased, may be directly observable in cold atoms experiments on low-dimensional systems.

Acknowledgments

B. P. van Zyl would like to acknowledge financial support from the Natural Sciences and Engineering Research Council (NSERC) of Canada through the Discovery Grants program. A. Farrell would like to acknowledge the NSERC Undergraduate Student Research Awards (USRA) program for additional financial support.

¹ A. B. Fowler, F. F. Fang, W. E. Howard, and P. J. Stiles, Phys. Rev. Lett. **16**, 901 (1966).

² *Solid State Physics: Semiconductor Heterostructures and Nanostructures*, (H. Ehrenreich and D. Turnbull ed.). Academic Press, New York, 1991.

³ P. Hohenberg and W. Kohn, Phys. Rev. B **136**, B864 (1964).

- ⁴ W. Kohn and K. Sham, Phys. Rev. B **140**, A1133 (1965).
- ⁵ L. H. Thomas, Proc. Camb. Phil. Soc. **3**, 542 (1927).
- ⁶ E. Fermi, Rend. Accad. Naz. Lincei. **6**, 602 (1927).
- ⁷ H. Eschrig, *Fundamentals of Density Functional Theory* (Teubner, Stuttgart, 1996).
- ⁸ R. M. Dreizler and E. K. U Gross, *Density Functional Theory: An Approach to the Quantum Many-Body Problem*, (Springer-Verlag, Berlin, Germany, 1990).
- ⁹ C. F. von Weizsäcker, Z. Phys. **96**, 431 (1935).
- ¹⁰ M. Brack and R. K. Bhaduri, *Semiclassical Physics*, Frontiers in Physics, Vol. 96 (Addison-Wesley, Reading, MA, 2003).
- ¹¹ A. Holas, P. M. Kozłowski, and N. H. March, J. Phys. A: Math. Gen **24**, 4249 (1991).
- ¹² L. Salasnich, J. Phys. A: Math. Theor. **40**, 9987 (2007).
- ¹³ M. Koivisto and M. Stott, Phys. Rev. B **76**, 195103 (2007).
- ¹⁴ B. P. van Zyl and E. Zaremba, Phys. Rev. B **59**, 2079 (1999); B. P. van Zyl and E. Zaremba, Physica E **6**, 423 (2000); B. P. van Zyl, E. Zaremba and D. A. W. Hutchinson, Phys. Rev. B **61** (2000); B. P. van Zyl and E. Zaremba, Phys. Rev. B **63**, 245317 (2001).
- ¹⁵ M. Brack, Phys. Rev. Lett **53**, 119 (1984).
- ¹⁶ H. Eschrig, Phys. Rev. B **82**, 205120 (2010).
- ¹⁷ The polylog function, $\text{Li}_2(\cdot)$ is identical to the Fermi integral, $F_\xi = \int_0^\infty \frac{\tau^\xi}{1+\exp(\tau-\eta)} d\tau$, with $\xi = 1$. See Ref. [10] for details.
- ¹⁸ J. Bartel, M. Brack, and M. Durand, Nucl. Phys. **A445**, 263 (1985).
- ¹⁹ The functional inversion procedure used here is not possible in 3D because of the complicated dependence of z and V on the spatial density. We refer the reader to Ref. [18] for a detailed derivation of the elimination of z and V in favour of ρ to obtain the 3D finite-temperature KE functional.
- ²⁰ P. Ring and P. Schuck, *The Nuclear Many-Body Problem*, (Springer-Verlag, Berlin, Germany, 2004).
- ²¹ While we have not presented the cumbersome calculation here, the more general result that *all* finite-temperature gradient corrections vanish at $T = 0$ has also been established.
- ²² M. Brack and B. P. van Zyl, Phys. Rev. Lett **86**, 1574 (2001).
- ²³ B. P. van Zyl, R. K. Bhaduri, A. Suzuki, and M. Brack, Rev. A **67**, 023609 (2003).
- ²⁴ P. Shea and B. P. van Zyl, J. Phys. A: Math. Theor. **40**, 10589 (2007).
- ²⁵ Wenhui Li, G. B. Partridge, Y. A. Liao, and R. G. Hulet, Int. J. Mod. Phys. B **23**, 3195 (2009).